



ELSEVIER

Contents lists available at ScienceDirect

Planetary and Space Science

journal homepage: www.elsevier.com/locate/pss

The geomorphology and morphometry of the banded terrain in Hellas basin, Mars



X. Diot^{a,b,*}, M.R. El-Maarry^c, F. Schlunegger^a, K.P. Norton^d, N. Thomas^{b,c}, P.M. Grindrod^{e,f}

^a Institut für Geologie Universität Bern, Baltzerstrasse 1-3 CH-3012 Berne, Switzerland

^b Center for Space and Habitability, Universität Bern, Sidlerstrasse 5 CH-3012 Berne, Switzerland

^c Physikalisches Institut, Universität Bern, Sidlerstrasse 5 CH-3012 Berne, Switzerland

^d School for Geography, Environment and Earth Science, Victoria University of Wellington, New Zealand

^e Department of Earth and Planetary Sciences, Birkbeck, University of London, London, UK

^f Centre for Planetary Sciences at UCL/Birkbeck, London, UK

ARTICLE INFO

Article history:

Received 4 February 2014

Received in revised form

24 June 2014

Accepted 26 June 2014

Available online 15 July 2014

Keywords:

Mars

Surface geology

Impact crater

Geomorphological processes

Flows

ABSTRACT

Hellas basin is a large impact basin situated in the southern highlands of Mars. The north-western part of the basin has the lowest elevation (-7.5 km) on the planet and contains a possibly unique terrain type, which we informally call “banded terrain”. The banded terrain is made up of smooth-looking banded deposits that display signs of viscous behavior and a paucity of superimposed impact craters. In this study, we use newly acquired high spatial resolution images from the High Resolution Imaging Science Experiment (HiRISE) in addition to existing datasets to characterize the geomorphology, the morphometry and the architecture of the banded terrain. The banded terrain is generally confined to the NW edge of the Alpheus Colles plateau. The individual bands are ~ 3 – 15 km-long, ~ 0.3 km-wide and are separated by narrow inter-band depressions, which are ~ 65 m-wide and ~ 10 m-deep. The bands display several morphologies that vary from linear to concentric forms. Morphometric analysis reveals that the slopes along a given linear or lobate band ranges from 0.5° to 15° (average $\sim 6^\circ$), whereas the concentric bands are located on flatter terrain (average slope ~ 2 – 3°). Crater-size frequency analysis yields an Amazonian-Hesperian boundary crater retention age for the terrain (~ 3 Gyr), which together, with the presence of very few degraded craters, either implies a recent emplacement, resurfacing, or intense erosion. The apparent sensitivity to local topography and preference for concentrating in localized depressions is compatible with deformation as a viscous fluid. In addition, the bands display clear signs of degradation and slumping at their margins along with a suite of other features that include fractured mounds, polygonal cracks at variable size-scales, and knobby/hummocky textures. Together, these features suggest an ice-rich composition for at least the upper layers of the terrain, which is currently being heavily modified through loss of ice and intense weathering, possibly by wind.

© 2014 Elsevier Ltd. All rights reserved.

1. Introduction

It is becoming widely accepted that liquid water formed lakes on the surface of Mars throughout its history (e.g., Cabrol and Grin, 2010). The current Martian climate is too low in temperature and pressure for liquid water to be stable over long periods although short-term stability is at least feasible (Haberle et al., 2001). Ponding of water occurs in local topographic lows and hence it is natural to ask whether there is evidence for ponding in the

topographically lowest areas on Mars, and likewise whether there is residual water (in the form of buried ice) in these areas.

The surface of Mars exhibits large variations in topography and also shows structures related to flows at many elevations (Squyres, 1979; Mangold and Allemand, 2001; Milliken et al., 2003; Morgan et al., 2009). For example, landforms possibly related to water–ice flow similar to glaciers on Earth have been identified at high elevations in the western Arsia Mons region (Head and Marchant, 2003). Lobate debris aprons, probably related to the presence of ground ice have been recognized in the fretted terrains of Deuteronilus Mensae in the dichotomy region in the northern hemisphere at intermediate elevations (Mangold, 2003; Morgan et al., 2009; Grindrod and Fawcett, 2011). In several places, Hellas basin displays diverse landforms and flow features attributed to

* Corresponding author at: Institut für Geologie Universität Bern, Baltzerstrasse 1-3, CH-3012, Switzerland.

E-mail address: xavier.diot@csh.unibe.ch (X. Diot).

the transport by liquid water or ice (Bandfield et al., 2008, 2013; Kostama et al., 2013; Zuschneid and van Gasselt, 2013). In the area of Dao Vallis and Harmakhis Vallis, debris aprons and viscous flow features are observed (Squyres, 1979; Crown et al., 1992, 2005; Milliken et al., 2003; Pierce and Crown, 2003; Hubbard et al., 2011). Layered deposits in the Terby Crater, located to the north of Hellas basin, have been interpreted by Wilson et al. (2007) and Ansan et al. (2011) as possible sub-aqueous deposits.

Here, we focus on Hellas basin (40°S, 68°E, Fig. 1) situated in the southern hemisphere, which is probably the oldest basin on Mars with an age around ~4 Gyrs (Werner, 2008) corresponding to the boundary between the pre-Noachian and Noachian periods (Nimmo and Tanaka, 2005). Thus, Hellas contains a long geologic record of fluvial, volcanic and eolian activity (Tanaka and Leonard, 1995). In addition, Hellas basin contains the lowest regions of Mars reaching depths greater than 7 km with respect to the reference datum (Smith et al., 1999). Because of this, Hellas represents a major catchment area (Bandfield et al., 2008, 2013). However, the substantial thickness of the atmosphere above Hellas and its high dusty aerosol content (Moore and Edgett, 1993; Cantor et al., 2001) makes it challenging to observe, which partly explains why the basin has a limited surface areal coverage by high-resolution imagers. Despite these difficulties, observations show that the basin's interior hosts an enigmatic unit in its deepest part that has been unofficially named "banded terrain" in previous studies (Thomas et al. 2010; El Maarry et al., 2012a). It is characterized by long, often thin, adjacent bands up to several kilometers long, which change orientation and warp, often in conjunction with local topography (Figs. 2 and 3). We suggest that the appearance of the bands may be a sign of viscous flow properties, something which we seek to test in this study.

The aim of this paper is to describe and characterize the banded terrain using both newly-acquired and currently available datasets to understand the terrain's morphometry and geomorphology at different size-scales, in order to gain an insight into its composition and depositional history. The depth of this region and its age combined with the possibility of long-distance sub-surface flow of water (Andrews-Hanna et al., 2007; Harrison and Grimm, 2009) suggests that NW Hellas might exhibit evidence of liquid

flow or periglacial processes, which we aim to test here using a combination of high-resolution images, morphometric investigations and geomorphic mapping.

2. Geologic setting

Hellas basin is approximately 3000 km-long, 1500 km-wide and 7 km-deep. It is one of the few places on Mars where temperatures and atmospheric pressures (~11.5 mbar) can regularly exceed the triple point of water during summer (Haberle et al., 2001), thereby allowing for transient stability of liquid water on the surface. Most of the interior of Hellas basin appears to be relatively young, displaying a low abundance of craters, and influenced by flows as indicated by the presence of viscous-flow features (Milliken et al., 2003; Hubbard et al., 2011).

The terrains surrounding Hellas basin as well as its interior may have been modified by the flow of water. In particular, Wilson et al., 2010 (see their Figure 7.1) mapped a network of valleys, which are present as meandering lineaments that terminate in the basin's interior. Thus they could have been the pathway for water that was collected upstream of Hellas from the surrounding highlands, and that finally discharged into the basin (Wilson et al., 2010). In addition, Moore and Wilhelms (2001) proposed that Hellas has experienced several lacustrine cycles in the past mainly because of the observation of white layers deposited along contours at different elevations, potentially indicative of ancient shorelines.

Moore and Wilhelms (2001, 2007)'s geological maps of Hellas and the surrounding terrains divides the interior of Hellas into five units: the smooth plains, the honeycomb terrain, the central plateau referred to as Alpheus Colles and the reticulate terrain. More recently, Thomas et al. (2010) and El Maarry et al. (2012a) identified and partially mapped a unit in the NW region of Hellas basin, which is the deepest part of Hellas: the banded terrain (35–43°S, 51–60°E, Figs. 1 and 10). This area is characterized by several morphological features with convolute forms consistent with the presence of a flowing material (Figs. 2–7). To the NW of the main topographic low

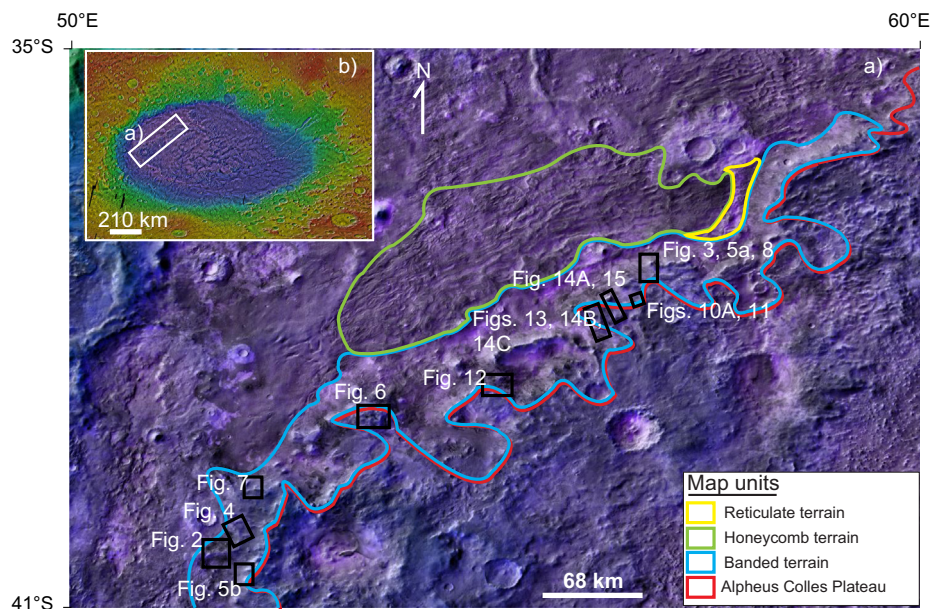


Fig. 1. (a) THEMIS day IR map overlaid with MOLA color elevation map of the NW Hellas basin (from Moore and Wilhelms, 2001, 2007) associated with (b) a general THEMIS day IR map overlaid with MOLA color elevation map to present the location of the study area (white box on the sketch b). The color outlines represent the different units for clarity. Colored outlines are: the Alpheus Colles plateau (red), the banded terrain (blue), the Honeycomb terrain (green), the reticulate terrain (yellow). The black boxes indicate the location of the other figures of this paper. (For interpretation of the references to color in this figure legend, the reader is referred to the web version of this article.)

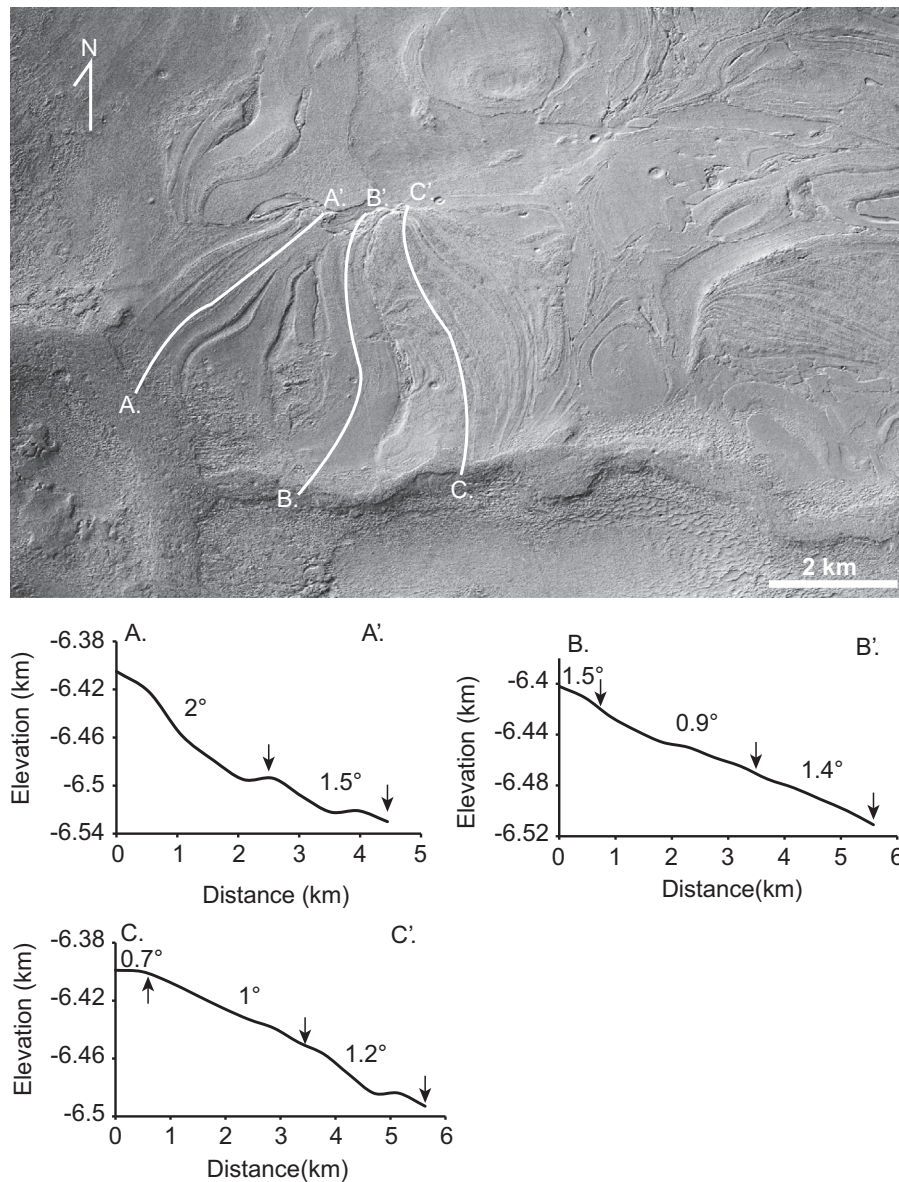


Fig. 2. Upper: CTX view (image ID: P17_007768_1371) showing linear bands (AA'–DD') (image center: 40.6°S, 51.5°E). White lines represent MOLA elevation profiles (AA'–DD'). Black arrows indicate the segments where the MOLA slope has been extracted (numbers 1.5°, 2° etc. between two arrows).

are the so-called honeycomb and the reticulate terrains (Moore and Wilhelms, 2001, 2007; Thomas et al., 2010; El-Maarry et al., 2012a). The honeycomb terrain is characterized by elliptic, polygonal shapes resembling cells or honeycombs that occasionally display raised rims and depressed interiors (Moore and Wilhelms 2001, 2007). The reticulate terrain consists of interconnected ridges parallel or tangential to the basin rim that form polygonal patterns (Moore and Wilhelms 2001, 2007). The boundaries between these two terrains are gradational, and the two terrains attain complex stratigraphic relations in some locations. North of the honeycomb terrain, a smooth and relatively flat terrain mapped as plain deposits (Moore and Wilhelms, 2001, 2007) marks the transition to a relatively steep flank that delineates the northern lateral border of Hellas basin. Southwest of the banded terrain, the Alpheus Colles plateau covers most of the center of the basin, rising ~1 km higher than the surrounding terrains (including the banded terrain). Moore and Wilhelms (2001, 2007) interpreted the Alpheus Colles plateau as thick multilayered deposits. The north-western edge of this plateau consists of a sinuous and relatively sharp boundary with the banded terrain (Figs. 1 and 10).

3. Datasets and methods

Our mapping and geological investigation was carried out using the datasets from the Context Camera (CTX, Malin et al., 2007) and the High Resolution Imaging Science Experiment (HiRISE, McEwen et al., 2007, 2010), which are both onboard on the NASA's Mars Reconnaissance Orbiter. CTX typically obtains 30 km-wide and 40 km-long images with a resolution of ~6 m/pixel. CTX was used to: characterize the architecture of the landscape, trace the spatial extent of the different units, identify stratigraphic boundaries, and to carry out a crater-size frequency analysis. The HiRISE camera has a much lower spatial coverage yet offers an ultra-high spatial resolution at 25–50 cm/pixel, which we use for detailed investigations of certain regions of interest as well as for identifying small-scale textures and landforms.

Elevation and morphometric analysis was carried out using the dataset from the Mars Orbiter Laser Altimeter (MOLA, Smith et al., 2001) onboard the Mars Global Surveyor, and Digital Terrain Models (DTMs) calculated from both CTX and HiRISE stereo images. MOLA provides an elevation map of the entire surface of

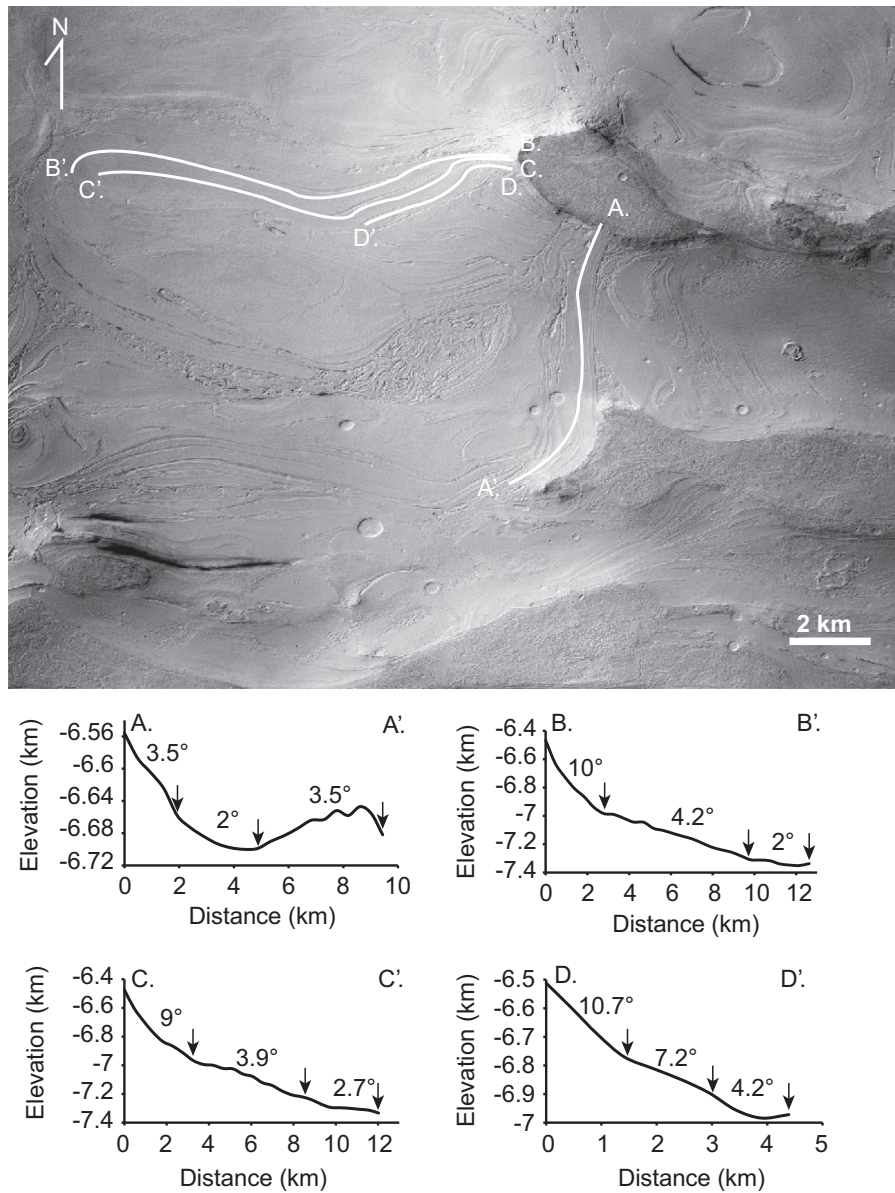


Fig. 3. Upper: CTX view (image IDs: P15_006924_1406, P16_007135_1417) showing linear bands (AA'–DD') (image center: 37.5°S, 56.8°E). White lines represent MOLA elevation profiles (AA'–DD'). Black arrows indicate the segments where the MOLA slope has been extracted (numbers 10°, 3.5° etc. between two arrows).

Mars with a horizontal resolution of 100 m. This map was used as a background for our mapping and as part of the geomorphic analyses. We made two CTX DTMs with spatial resolutions of 20 m/pixel, using standard methods involving the ISIS and BAE Systems SocetSet software (Kirk et al., 2008). By following previous methods (e.g. Kirk et al., 2008; Okubo, 2010; Grindrod et al., 2012) we estimated the vertical precision of our CTX DTMs to be 2.1 and 2.7 m for the image pairs G18_025147_1407 – G18_025437_1406 and G19_025648_1419 – G20_025925_1419, respectively. We also utilized a 1 m/pixel HiRISE stereo DTM (DTEEC_007491_1405_007201_1405_U01) archived in the Planetary Data System (PDS), for which we estimated a vertical precision of 0.5 m. These DTMs were used to generate relief and slope maps as well as 3-dimensional views.

The final maps were constructed within a GIS environment using JMARS (<http://jmars.asu.edu>, Gorelick et al., 2003) and ArcGIS (<http://www.esri.com/software/arcgis>), which allows the combination of multiple datasets including elevation, slope patterns, volumes, relief, aspect ratios, etc. The 3-dimensional views

were constructed within the GIS environment Global Mapper (<http://www.blumarblegeo.com/products/global-mapper.php>). The crater-size frequency analysis was carried out using the available Craterstat2 tool (<http://hrscview.fu-berlin.de/craterstats.html>, Michael and Neukum, 2010).

4. Results

We identified four distinct geomorphic domains in the NW interior of Hellas based on the morphological shape of the terrains: the Alpheus Colles plateau, the banded terrain, the honeycomb terrain and the reticulate terrain (Figs. 1 and 10). Some morphological descriptions of these terrains such as the Alpheus Colles plateau, the honeycomb terrain and the reticulate terrain were already presented by Moore and Wilhelms (2001, 2007). However, using recent CTX and HiRISE images, we were able to expand on these earlier mapping efforts and identify finer surface textures and morphologies.

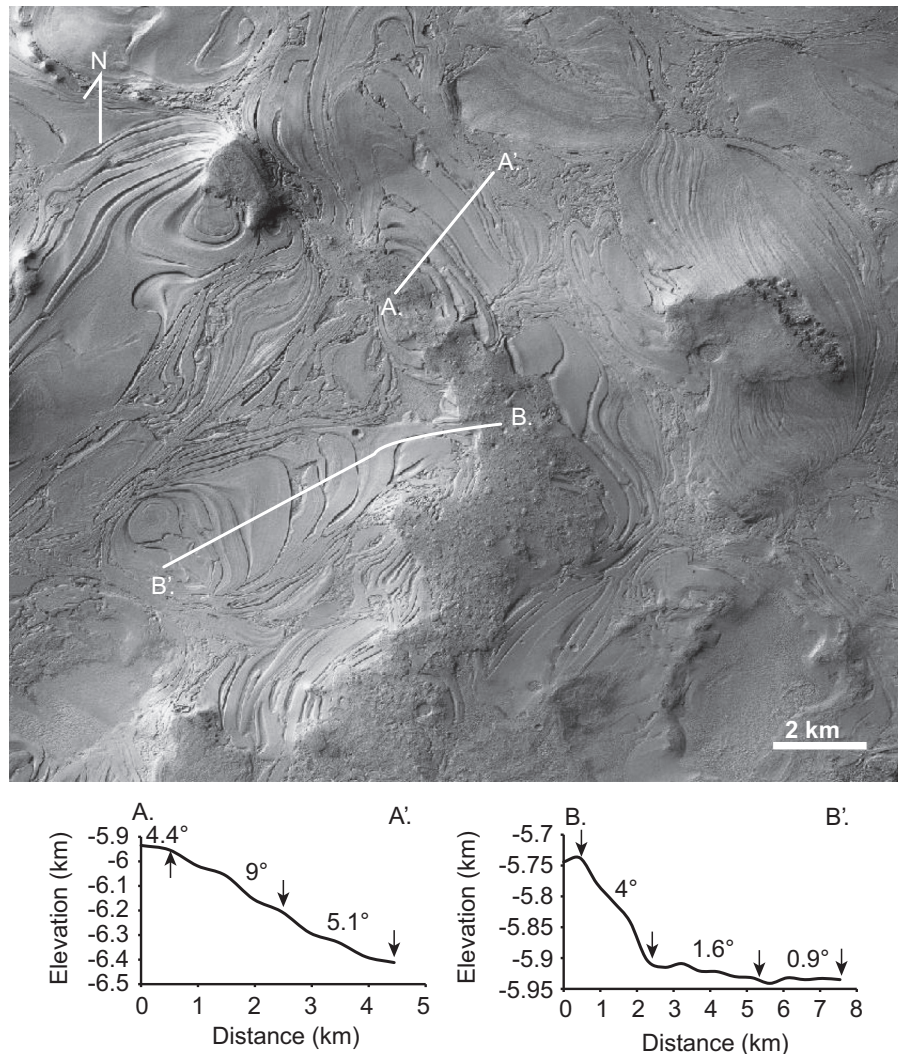


Fig. 4. Upper: CTX view (image IDs: B18_016642_1371) showing lobate bands (AA'–BB') (image center: 40.4°S, 52.3°E). White lines represent MOLA elevation profiles (AA'–BB'). Black arrows indicate the segments where the MOLA slope has been extracted (numbers 9°, 4° etc. between two arrows).

4.1. Surface morphology

The banded terrain displays alternating small relief, resembling bands and small depressions referred to as inter-bands (Figs. 2–7). The measurements of > 300 bands yield lengths that range from 3 to 15 km (average ~5 km) and widths between 90 and 1000 m (average ~320 m). The inter-bands are characterized by similar lengths as the bands they separate, with widths that range between 10 and 90 m (average around 65 m). The band features display a variety of shapes including linear, lobate, and closed concentric forms with the dimensions described above (Diot et al., 2013, Figs. 2–7 and 11). The linear bands (Figs. 2 and 3) are localized mostly on the slopes of the NW edge of the Alpheus Colles plateau and locally on the top of the plateau (Figs. 1, 10 and 11A). These latter bands are characterized by smooth, curved and streamlined shapes, exhibiting varying orientations (Figs. 2, 3 and 8 and red lines on 11B). In most cases, the curves are constrained by the surrounding topography as is the case illustrated in Fig. 3 where the linear band A–A' swings around the local heights at its termini. In addition, most of the linear bands are situated east of the concentric bands (Fig. 11A). Generally, the linear bands and the inter-bands initiate at topographic heights (extremities A, B, and C on Fig. 2, extremities A, B, C and D on Fig. 3 and 8). Some of these bands originate at the margin of the uneven and sinuous NW

boundary of the Alpheus Colles plateau, which is consistent with an erosive origin for this boundary (Figs. 1, 10 and 11B). Such linear bands end with a distinct terminal point at lower elevations (extremities A', B', and C' on Fig. 2, extremities A', B', C' and D' on Figs. 3 and 8). Likewise, the lobate bands initiate at relatively high topographic points and show distinct termini (Figs. 4, 5, 8 and 11B). Finally, most of the concentric bands are located close to the honeycomb terrain. They are also present in local depressions (Figs. 6–8 and 11A). The long axis of the concentric closed bands displays several orientations, but the E–W trend appears to predominate.

4.2. Crater retention age

The determination of the banded terrain's crater retention age was achieved using crater-size frequency analysis. The CTX images allowed the counting of craters down to 20 m in diameter. The large size range was selected in order to obtain an accurate date of emplacement, investigate possible resurfacing, and assess the terrain's crater retention properties. Since the banded terrain is well-defined in terms of spatial extent (~12,000 km²), the counting was carried out on the entire unit. The largest craters encountered were ~3 km-wide. The state of preservation of craters is variable. Some craters display well-defined rims, while others have eroded rims and contain variable

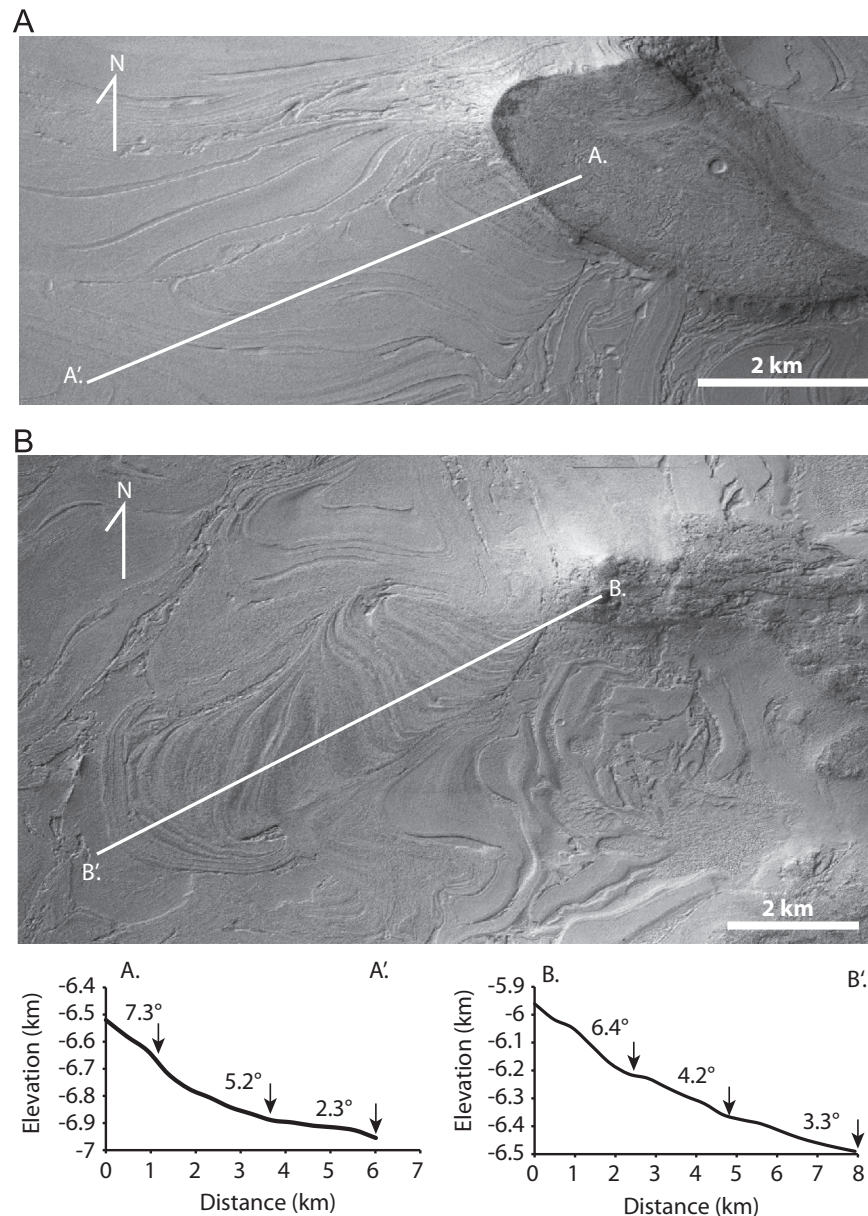


Fig. 5. Upper: (a) Lobate bands (AA') (image IDs: P15_006924_1406, image center: 37.7°S, 56.9°E). (b) Lobate bands (BB') (image IDs: P17_007768_1371, image center: 41.4°S, 51.7°E). White lines represent MOLA elevation profiles (AA'–BB'). Black arrows indicate the segments where the MOLA slope has been extracted (numbers 7.3°, 4.2° etc. between two arrows).

amounts of crater-fill material. Finally, a slight E-W elongation (less than 2%) is observed for some craters but overall, evidence for large post-impact modification is small to negligible.

Our crater-size frequency analysis employed a total crater population of ~3000 craters (Fig. 9). Generally, the crater densities do not fall on unique isochrones. The largest craters (> 2 km-wide) yield a probable emplacement age of ~3.1 Gyr, albeit with large error bars due to the small number of craters used for the age determination. The craters in the 0.9–2 km-range display more consistency and after making corrections to account for potential resurfacing (Michael and Neukum, 2010) yield an age of ~2.9 Gyr. The rest of the craters (< 0.9 km-wide) show preferential removal of the smaller crater population and cannot be used to derive ages of possible subsequent resurfacing with a high degree of certainty. The distribution of plotted crater densities could be attributed to (a) intense weathering (possibly by wind erosion) preferentially resulting in the abrasion of small craters, (b) resurfacing events that erode the smaller populations, or (c) poor-crater retention ability for the materials comprising

the terrains. Therefore, we consider the oldest age derived from our crater plots (~3 Gyr) to be a minimum age of emplacement for the banded terrain. This age estimate is slightly younger than Mangold et al. (2012)'s estimate of ~4 Gyr for the formation of Hellas Basin. Interestingly though, the emplacement age of the banded terrain is comparable to Mest and Crown (2001)'s estimate of upper Hesperian to middle Amazonian age for the icy landforms such as the lobate debris aprons located in the east of Hellas.

4.3. Morphometry

We have extracted 15 MOLA elevation profiles oriented SE–NW in the banded terrain using JMARS. Here we present two of them, which are characteristic of the topography in the NW interior of Hellas (Fig. 10). The banded terrain is located downslope in a trough to the NW edge of the Alpheus Colles plateau and in some local depressions on the top of this plateau (Figs. 10 and 11A). This trough is approximately 50 km wide with a maximum depth of

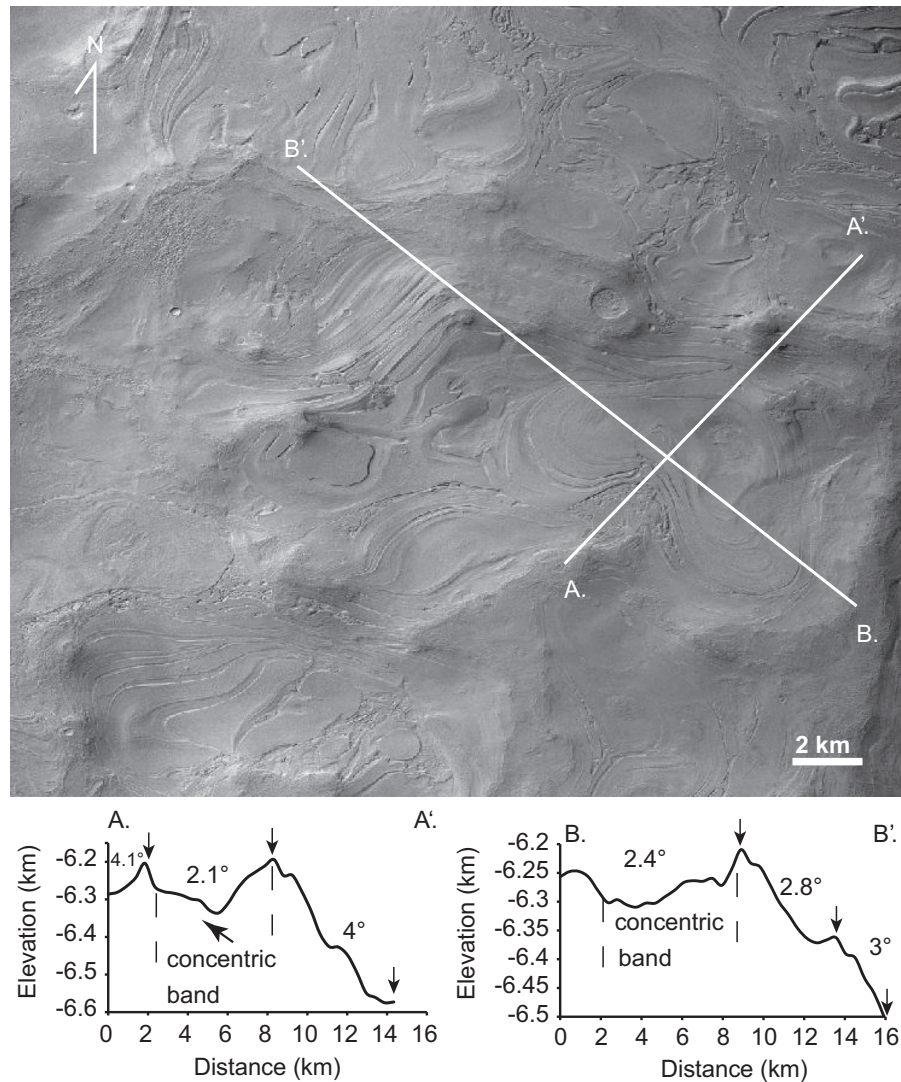


Fig. 6. Upper: Concentric bands (image IDs: P17_007557_1386, image center: 39.4°S, 53.2°E). White lines represent MOLA elevation profiles (AA'–BB'). Black arrows indicate the segments where the MOLA slope has been extracted (numbers 2.1°, 4° etc. between two arrows).

around 7.5 km in relation to MOLA's reference datum (profiles AA' and BB' on Fig. 10), which represents the lowest region on Mars. The associated honeycomb terrain and reticulate terrain are situated to the north of the banded terrain on a plateau of nearly constant elevation of -7 to -7.4 km, approximately 200–500 m higher than the lowest point where banded terrain is located (profiles on Fig. 10).

MOLA slopes and elevation profiles (Figs. 2–7) along linear bands (70 measurements, 7 profiles presented here), perpendicular to the lobate (20 measurements, 4 characteristics profiles presented here) and concentric bands (70 measurements, 2 characteristics profiles presented here) have been produced to precisely quantify the morphology of the banded terrain structures. The MOLA elevation profiles along linear bands show a convex topography on most of the profiles within the first two kilometers followed by a concave topography and some steps (Figs. 2 and 3). The slope is variable along the linear bands but generally decreases towards the bands' termini except where local mounds are present along the bands (e.g., profile AA' in Fig. 3). The higher parts of the linear bands display slopes that range between 0.7° to 15° with an average around 6° , whereas at the termini, or lower parts of the linear bands, the slopes vary between 0.5° and 4° with an average of $\sim 2^\circ$ (Figs. 2 and 3). The MOLA elevation profiles perpendicular to the lobate bands show a convex topography

within the two first kilometers followed by either a concave, or a flat topography (Figs. 4 and 5). Slopes tend to decrease from the higher part (4 – 9° with an average of 6°) to the lower part (0.9 – 5° with an average of 2.5°) of a given lobate band (Figs. 4 and 5). Two MOLA slope and elevation profiles in two different directions have been acquired for each given concentric band (Figs. 6 and 7): one following the long axis of the band (profiles BB' on Figs. 6 and 7) and one following the short axis (profiles AA' on Figs. 6 and 7).

The shape of the concentric band is strongly dependent on the surrounding topography. As observed in Figs. 6 and 7, the concentric bands are located in local concentric depressions delimited by crests or ridges. It should be noted that the relative elongated shape along the long axis of the concentric band on Fig. 7 is due to the convex shape of the topography because of the lack of topographic heights at the extremity B' (profile BB' Fig. 7). The slope along the two axes is relatively homogeneous, with an average around 2 – 3° , which is lower than the values observed in the other band morphologies (linear and lobate). The E–W alignment of the concentric bands and the orientation of the lobate bands tend to be nearly perpendicular to the direction of the main slope, whereas the linear bands are parallel to the direction of the main gradient.

We used HiRISE and CTX DTMs to compute in detail the slope and the local relief. The relief of the inter-bands is extracted using

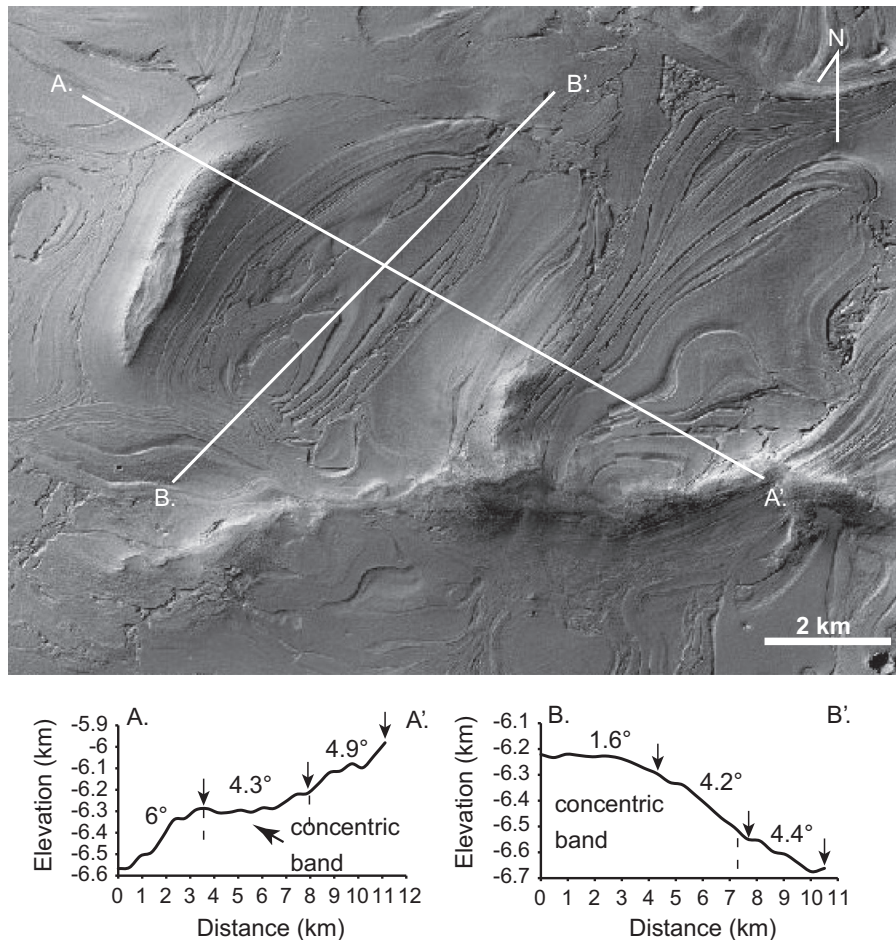


Fig. 7. Upper: Concentric bands (image IDs: P17_007768_1371, P18_007913_1371, image center: 40.3°S, 51.9°E). White lines represent MOLA elevation profiles (AA'–BB'). Black arrows indicate the segments where the MOLA slope has been extracted (numbers 6°, 4.4° etc. between two arrows).

the generated relief maps (Fig. 12), where it quantifies the difference in elevation between two points (Ahnert, 1984). In our relief maps, the highest point represents the surface of the bands and the lowest point is the surface of the inter-bands. We used sliding windows sizes of 40 m × 40 m, 80 m × 80 m and 100 m × 100 m, which are dynamic cells moving horizontally on the DTMs, with an overlap of the edges of the sliding windows. At each iteration, the maximum elevation of the DTM is assigned to the center of the cell and we finally obtain a surface of maximum elevation (maximum topographic envelope) (Grohmann and Riccomini, 2009). Subtraction of this maximum elevation surface by the DTM, which reflects the surface topography, yields a minimum relief for the inter-bands (Fig. 12). Multiple relief profiles were created to quantify the relief of the inter-bands more precisely. The results yield a relief of at least 10–12 m for the inter-bands at this scale (Fig. 12). These values compare well with similar estimates of 10–15 m using lengths of shadows on HiRISE images, which were studied as well in order to verify our estimates and extend our analysis to regions not covered by our DTMs.

4.4. Surface texture of the banded terrain using HiRISE

The HiRISE images (25 images analyzed) reveal differences in the surface texture between the bands and the inter-bands. The bands show a pitted or hummocky surface with meter-sized boulders distributed over the entire bands' surface. The inter-bands display possible dunes of dusty material that have accumulated in the natural depressions and smooth surfaces (Fig. 13). In addition, numerous structures and features are observed on the surfaces of the bands.

These include polygonal surface patterns, fractured mounds and signs of progressive degradation in the boundaries of several bands (Figs. 14 and 15).

Surface patterns are abundant in the banded terrain and form polygonal patterns of different sizes. Two main size-ranges are observed: a small-sized group ~10 m-wide polygons and a second group that displays larger polygons sizes with a range of 20–60 m. The larger polygons display high centers and bounding troughs, while the small polygons have low centers and bulging edges (Fig. 14B). Both sets of polygons appear together in many locations, and the smaller appear to overlie the larger ones. Indeed, in some locations relics of larger polygons are observable below small polygons (Fig. 14B). The fractured mounds (Fig. 14A) are typically 20–50 m-wide and 2–8 m-high (using length of shadows). Fractures present on the top of certain mounds have no preferential directions. Generally, the mounds are spatially associated with the polygons.

Finally, in some places, a degradation of the bands is observed (Fig. 15). This degradation appears to be progressive because of the decrease in size of the material's blocks with increasing distance from the bands. Indeed, the relief of the blocks close to the bands is between 1.5 m and 3 m with an average around 2 m, while the relief of the blocks decreases to approximately 1 m away from the bands.

5. Discussion

The high spatial resolution datasets used here show that the banded terrain consists of alternating bands and narrow inter-bands

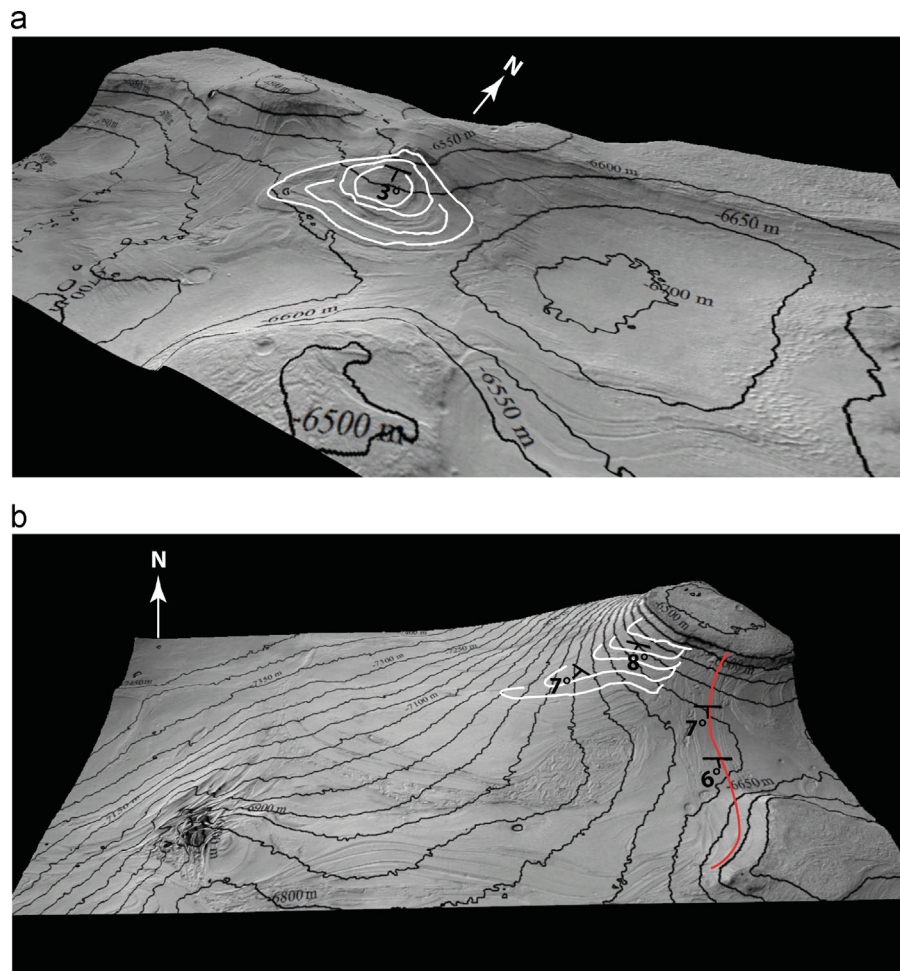


Fig. 8. 3 Dimensional (3D) views from CTX DTM (built from the pair of CTX image IDs: G19_025648_1419 – G20_025925_1419) for the different shapes of banded terrain. (A) the concentric bands (white line). The vertical exaggeration of this 3D view is 7; (B) the linear bands (red line) and the lobate bands (white line). The vertical exaggeration is 5. (For interpretation of the references to color in this figure legend, the reader is referred to the web version of this article.)

depressions or troughs. The banded terrain displays three main forms: (1) linear bands with sinuous morphology and long axes that run parallel to the local slope, (2) lobate bands that have their long axis perpendicular to the slope, and (3) concentric bands that fill local depressions with long axes perpendicular to the slope and texture that is identical to the other bands. In addition, HiRISE images have resulted in the identification of small meter-scale features including polygonal surface patterns, fractured mounds and evidence for progressive degradation at the boundaries of many bands. In the following sections, we use these observations to discuss the structures observed at high spatial resolution along with their implications, the flow-like behavior, and possible composition of the banded terrain.

5.1. Observations of structures possibly related to ice-rich materials

The polygonal surface patterns (Fig. 14B) observed on bands close to the NW edge of the Alpheus Colles plateau is possibly indicative of ice-rich material in the banded terrain. Indeed, thermal contraction can lead to the formation of polygonal cracks in frozen soils (e.g., Mellon, 1997; Mangold, 2005; Levy et al., 2010). However, other processes could also be responsible such as desiccation or tectonic jointing (El Maarry et al., 2010, 2012b) yet are less likely. In the case of thermal contraction, the cracks may persist because freeze-thaw cycles would result in an enlargement of the cracks (Fig. 14B). In this context, the rectilinear form of the larger polygons (the 20–60 m-wide) can be explained as

geomorphic response to anisotropic stress fields that are common on sloped regions (Lachenbruch, 1962). Likewise, we consider the fractured mounds (Fig. 14A) to have developed through freeze/thaw cycles of water ice. In this case, the growth of ice lenses in the near subsurface creates mounds or small bulges that may exhibit cracks on the surface of the mounds. As such, the presence of these features is indicative of a periglacial landscape, which bears close similarities to other regions on Mars such as Utopia Planitia. This latter area also shows a suite of periglacial-like features that include surface polygonal patterns (Levy et al., 2009, 2010; Séjourné et al., 2011; Lefort et al., 2005, 2010) and fractured mounds (Dundas and McEwen, 2010; Soare et al., 2013). The occurrence of periglacial structures have also been inferred in the Peneus Patera and Amphitrites Patera regions to the south of Hellas (Lefort et al., 2005, 2010). Finally, the degradation of the bands into distinct blocks (Figs. 14C and 15) could be caused not only in response to freeze/thaw cycles of ice but also by the sublimation of ice. Indeed the degraded area has a hummocky surface texture that is analogous to what Levy et al. (2009) informally named as “brain terrain” in the Utopia plains. These authors proposed that this surface texture was formed by the sublimation of ice. In addition, eolian abrasion of the friable desiccated materials that are no longer ice-rich (see Howard et al., 2012) could be responsible for bands' degradation. It should be noted that these features are strongly indicative of an ice-rich composition for the upper layers of the banded terrain but may not necessarily indicate a main bulk composition. In the next

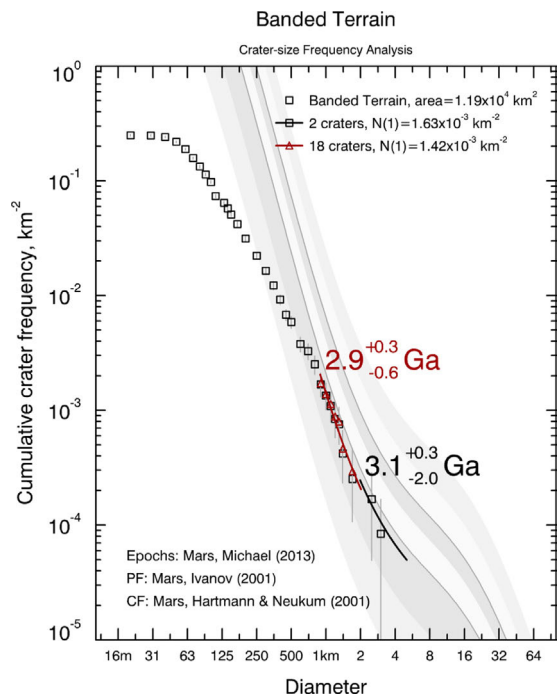


Fig. 9. Cumulative crater counts in the banded terrain ($\sim 12,000 \text{ km}^2$). Black squares show the data, the red line represents the best fit for craters in the 0.9–2 km range and the black line represents the best fit for the larger crater giving the oldest crater retention age. (For interpretation of the references to color in this figure legend, the reader is referred to the web version of this article.)

section, we discuss if the banded terrain is composed mainly of ice-rich materials, or whether it should be rather considered as an upper ice-rich layer/mantle unit.

5.2. Main composition and formation mechanism of the banded terrain

The observed sinuous streamline forms with smooth changes in direction (Figs. 2–7 and 8) suggest the presence of materials that undergo plastic deformation where strain rates are a function of pressure, stress gradients and the dynamic viscosity (Allen, 2009). The deforming material could correspond to one single component (e.g., ice, salt, lava) or a composition of two or more materials where at least one component is allowed to experience plastic deformation under conditions prevailing on Mars. This could be an assemblage of rock fragments with plastic material in the pore space where the latter most likely formed the supporting framework of the bands, allowing plastic flow to occur. Alternatively, it is also possible that the rock particles and the inferred plastic material formed a stratified architecture where the former rested on top of the plastic component.

The presence of many small non-deformed craters on the bands suggests that the materials are no longer flowing or deforming. Moreover, the terminal points (lower edges) of the linear and lobate bands are generally located on slopes ($\sim 2\text{--}3^\circ$ with some cases at 4°) (Figs. 2–5) and not on flat terrains. The position of these terminal points suggests that the linear and lobate bands are “frozen” on the slope, which suggests that the emplacement of the material is limited by threshold conditions regarding stress patterns. This is most commonly observed in materials where deformation is accomplished by lateral dislocation and/or diffusion creep of an assemblage of crystals (Goldsby and Kohlstedt, 1997, 2001), thus constraining the plastic material to a solid phase with a crystalline structure as is observed in e.g., ice. In addition, the tongue shapes of the linear or lobate bands is analogous to terrestrial glaciers and viscous flow features on Mars

including lobate debris apron (e.g., Squyres, 1979; Mangold, 2003; Milliken et al., 2003; Hartmann et al., 2014). These have been interpreted to be ice-rich landforms by various techniques that include geomorphological analysis, modeling, and radar measurements (e.g., Mangold and Allemand, 2001; Head et al., 2005, 2006; Plaut et al., 2009).

In the framework of this hypothesis, it has been postulated that ice starts to flow when the basal stress (τ_b) has exceeded the plastic limit (Paterson, 1981, Mangold and Allemand, 2001, Hartmann et al., 2014). The basal stress (τ_b) is defined by the following equation:

$$\tau_b = \rho g h \tan \theta,$$

where θ is the slope of the detachment horizon beneath the ice, h and $\rho = 920 \text{ kg/m}^3$ correspond to the ice's thickness and density, and g is the Martian's gravity where $g_{\text{mars}} = 3.72 \text{ m/s}^2$. In our case, the consideration of an average slope around 6° and a thickness h in a range of 12–30 m for the linear and lobate bands (Fig. 12) yields a minimum basal stress of 4.3–10 kPa, which is much lower than the threshold values of 100–300 kPa (Whalley and Martin, 1992) and 50–100 kPa (Paterson, 1994; Mangold and Allemand, 2001; Hartmann et al., 2014) estimated for terrestrial rock glacier and ice glaciers, respectively. Likewise, our range of basal stresses is substantially lower than the values (30–80 kPa) calculated for lobate debris aprons on Mars (Mangold and Allemand, 2001; Hartmann et al., 2014). However, if we calculate the basal stresses for the steepest linear and lobate bands where maximum hillslope angles are nearly 15° and where the both bands are up to 30 m thick, we obtain a basal stress around 28 kPa. This value is slightly lower than the lower bound calculated for the lobate debris apron (Mangold and Allemand, 2001; Hartmann et al., 2014). This can be explained by the fact that the ice can deform at low temperature and low stresses (De La Chapelle et al., 1998; Mangold and Allemand, 2001). Such scenario is not unlikely for explaining the displacement of the steepest bands. Hellas is the deepest part on Mars thus the temperatures can reach very low values, which in turn favors the plastic deformation of ice at such low stresses (e.g. Mangold and Allemand, 2001). In addition, Li et al. (2005) showed that after an extended period of time, a significant amount of ice is expected to sublimate, which would lead to a deviation in the debris aprons' longitudinal MOLA profile from the theoretical plastic model profiles (see their Fig. 6). This would imply that the actual topography may not be that of the initial flows, which would suggest that our calculations of the basal stresses yield minimum estimates. As the material's thickness decreases (by sublimation or wind abrasion), or alternatively, as the terrain becomes flatter, the downslope displacement decreases, and the material comes to a halt. In addition, the slope variations observed on the profiles and the presence of knick points (Figs. 2–5) indicate a chaotic aspect of the terrains, which may have controlled the changes of the bands' preferred orientation. However, this mechanism of pure ice deformation fails to explain the formation of the bands in the flatter regions where basal shear stress are between 4.3 kPa and 10 kPa.

Another constraint to the “pure-ice” hypothesis is the fact that the banded terrain displays features that are not analogous to other “viscous flow features” on Mars in terms of size, variable morphologies, bands-inter-bands patterns, slopes, etc. Therefore, more in-depth work is needed to understand why these features are uncommon on Mars and appear to be confined to a specific region in the Hellas basin. Alternatively, lava flows could form structures analogous to the ones of the linear bands. However, we tentatively abstain from this interpretation because of a lack of evidence of volcanic source regions (Thomas et al., 2010), or dykes resulting from the vertical intrusion of lava. It should be noted that evaporite-rich deposits can also create flow-like morphologies if

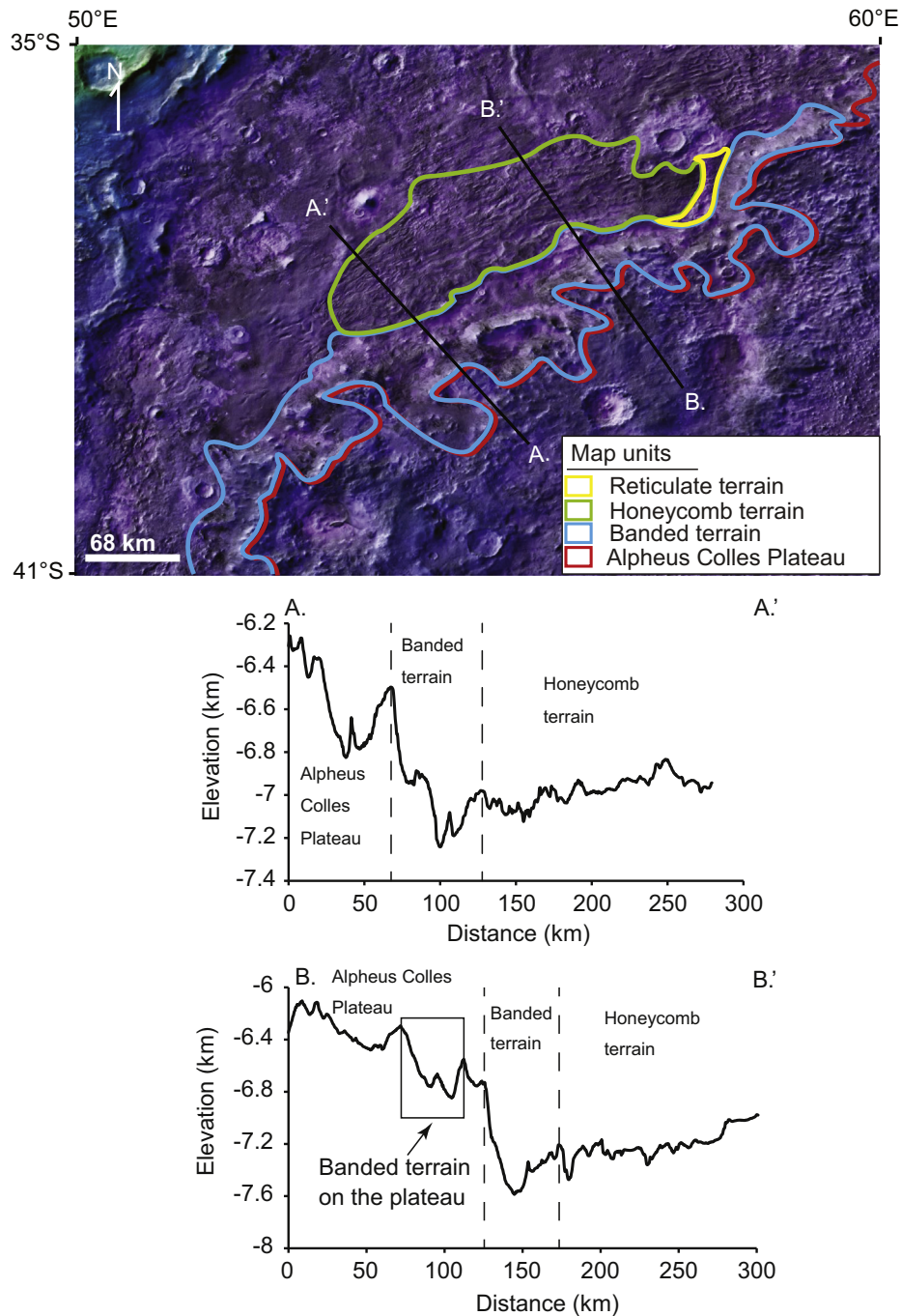


Fig. 10. THEMIS day IR map overlaid with MOLA color elevation map of Hellas basin associated with two MOLA elevation profiles (AA' and BB'). The color outlines represent the units of interest for clarity. Colored outlines are: the Alpheus Colles plateau (red), the banded terrain (blue), the Honeycomb terrain (green), the reticulate terrain (yellow). (For interpretation of the references to color in this figure legend, the reader is referred to the web version of this article.)

the deposits act as diapers enclosed in higher density materials for prolonged times – a hypothesis that has already been suggested before for the banded-reticulate-honeycomb landscape assemblage (Mangold and Allemand, 2003). However, the banded terrain deposits do not show evidence of doming as is common in diapiric evaporite deposits on Earth and other salt dome candidates on Mars (e.g., Baioni and Wezel, 2010). Moreover, soft deformation of salt deposits occurs at temperatures of only 100 °C and the layers of the overburden over diapers should display brittle deformation as it is the case on Earth (Mangold and Allemand, 2003). Our close inspection of the available HiRISE images does not show any signs for such brittle deformation in the banded terrain. Therefore, we find the salt diaper hypothesis

unlikely in view of our current investigation, especially in the absence of spectral information for the surface. Finally, we note that Howard et al. (2012) recently pointed towards eolian erosion as a relevant process that might explain some of the morphologies observed in our region and the honeycomb terrain (in fact, Howard et al. refer collectively to the region containing both the honeycomb and banded terrains as “honeycombs” or unit HT). In their study, they used mesoscale circulation models to suggest that strong katabatic winds would lead to at least 1 km of erosion in the deepest areas in Hellas basin. Such a scenario could solve some of the drawbacks (ice thickness below threshold conditions) related to the ‘pure ice’ hypothesis for explaining the displacement of the banded terrain in the flatter areas (see above). Our

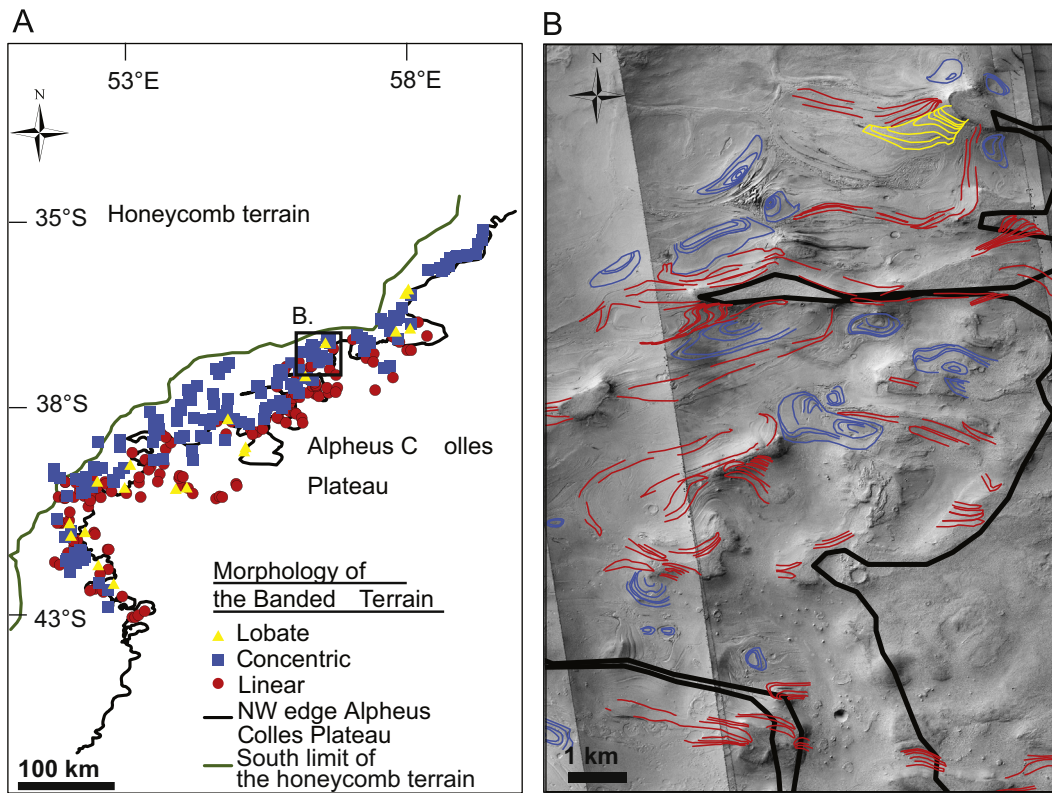


Fig. 11. (A) map of the location of the different shapes of banded terrain and (B) Structural map (centered at 56.6°E, 37.8°S) of the banded terrain based on CTX images (image IDs: G20_025925_1419, P16_007135_1417). Colors on (B): the linear bands (red lines), the concentric bands (blue lines), the lobate bands (yellow lines) and the NW edge of the Alpheus Colles (black line). Colored features on (A): linear bands (red dots), concentric bands (blue squares), lobate bands (yellow triangles), the southern boundary of honeycomb terrain (green line) and the NW edge of the Alpheus Colles plateau (black line). (For interpretation of the references to color in this figure legend, the reader is referred to the web version of this article.)

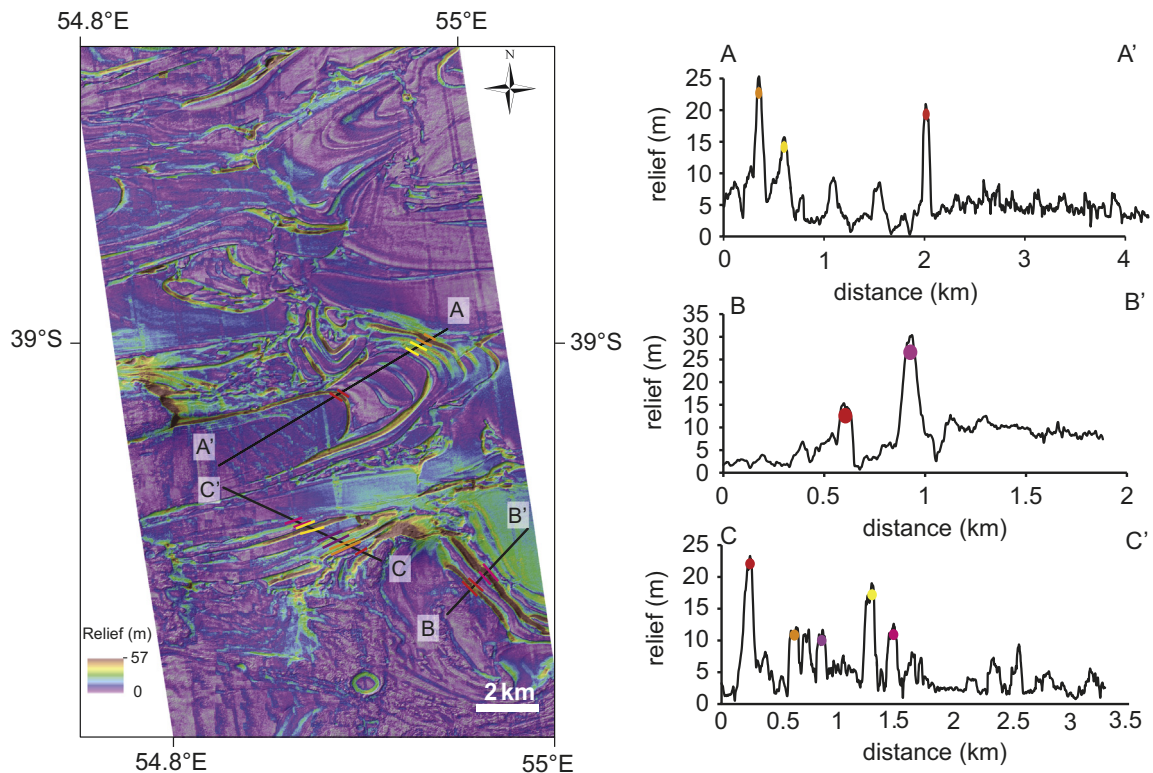


Fig. 12. Relief map (left) from HiRISE DTM associated with profiles (right: A–A', B–B' and C–C'). DTM built from the HiRISE images pair: PSP_007201_1405–PSP_007491_1405. The colored dots on the relief profiles correspond to the intervals of the same color on the map. (For interpretation of the references to color in this figure legend, the reader is referred to the web version of this article.)

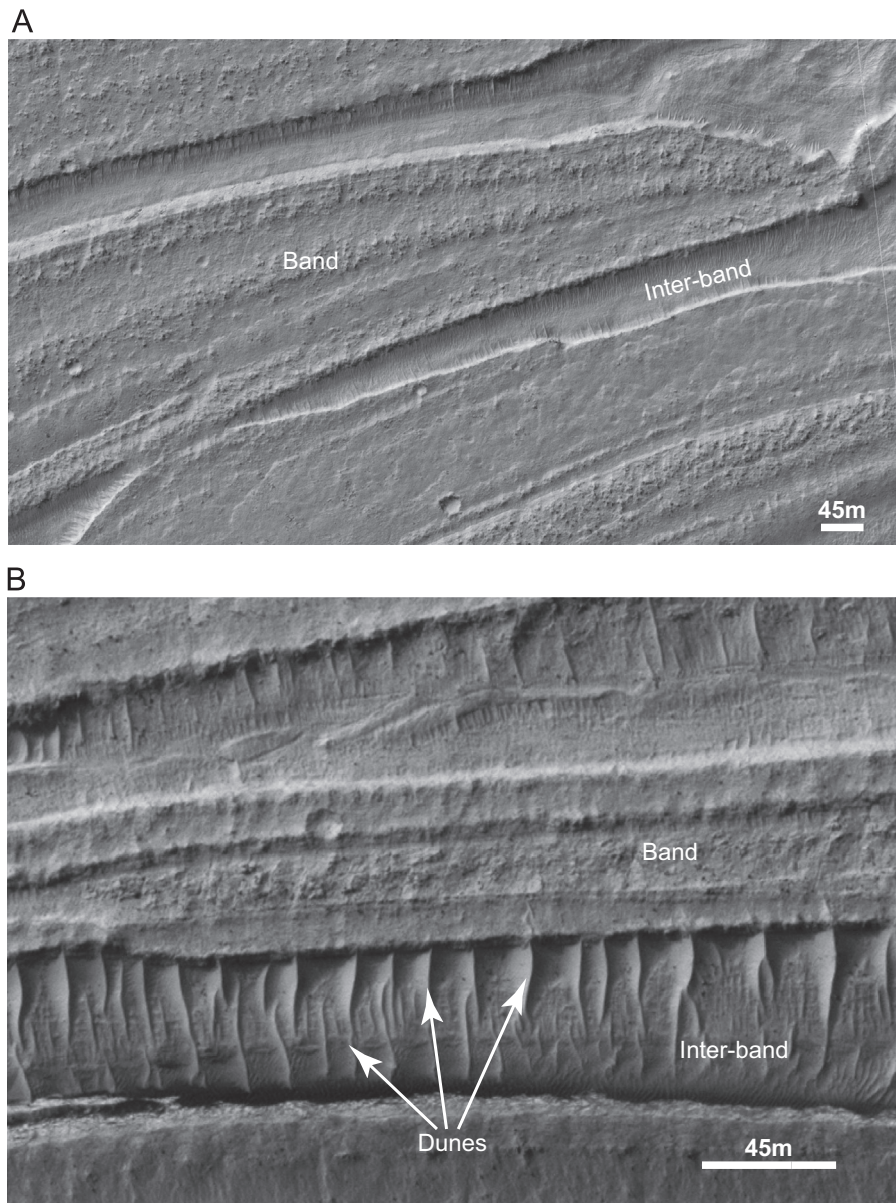


Fig. 13. (A) Example of the pitted or hummocky surface of the bands (view centered at 38.3°S, 56.3°E). (B) The relative smooth surface with possible dunes of the inter-bands (view centered at 38.4°S, 56.2°E). Both are observed on HiRISE image (image ID: PSP_007570_1415).

observations, particularly those of the banded terrain degradation, are consistent with Howard et al. (2012)'s predictions of intense erosion. However, the differences in the orientations of the surface textures that we have identified for the bands and inter-bands are inconsistent with a scenario of eolian degradation. In addition, it is difficult to reconcile it with the absence of dust mantling and the rarity of surface expression of eolian erosion in the region (Howard et al., 2012) except for limited observation of potential mega-ripples in depressions, which we assume are similar to our observations of dune-like materials in the inter-bands. Therefore, we conclude that eolian erosion could indeed be a possible modifying process in the shaping of the banded terrain but is not the main mechanism of initial formation.

6. Conclusion

In this study we used a geomorphological approach to characterize the banded terrain and investigate the composition of the

banded terrain. Our geomorphological map of the interior of NW Hellas shows several domains. Among them, the banded terrain covers a large band (35–42°S, 51–60°E) close to the NW edge of the Alpheus Colles plateau.

The general banded terrain structure consists of alternating small reliefs (bands) and small depressions (inter-bands). Morphologically, the banded terrain displays a variety of shapes comprising linear, lobate, and closed concentric forms. The linear bands, starting at high topographical points and ending at distinct terminal points, display multiple smooth changes in directions. The lobate bands, presenting a succession of lobes, also start from high topographical points. The concentric bands' shapes are oriented generally E–W and situated on terrain flatter than the linear bands and lobate bands. The relief analysis provides an inter-band relief of at least 12 m. The dating by crater counting yields an average age of ~ 3 Gyr corresponding to Amazonian–Hesperian boundary. Due to the sinuous streamline shape and the position in the slope (~ 2 – 3°) of the terminal points, we suggest that the linear and lobate bands could have been formed by

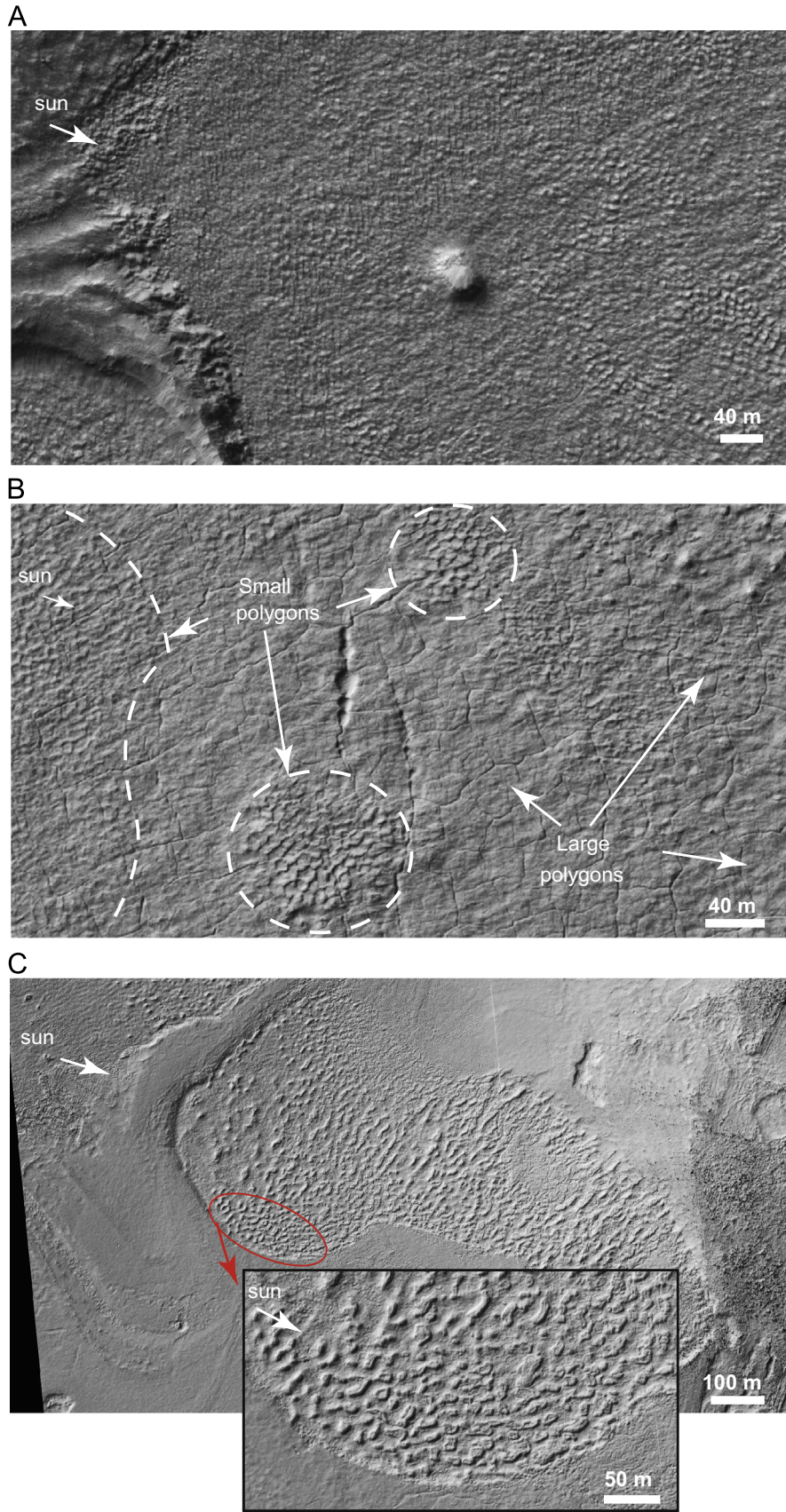


Fig. 14. HiRISE images showing the different structures possibly related to ice rich material. (A) Fractured mound (image ID: ESP_025925_1420, located at 37.8°S, 56.8°E); (B) Small and large polygons (image ID: PSP_007570_1415, located at 38.19°S, 56.21°E) and (C) Area analog to the “brain terrain” in Utopia plains (image ID: PSP_007570_1415, located at 38.25°S, 56.2°E).

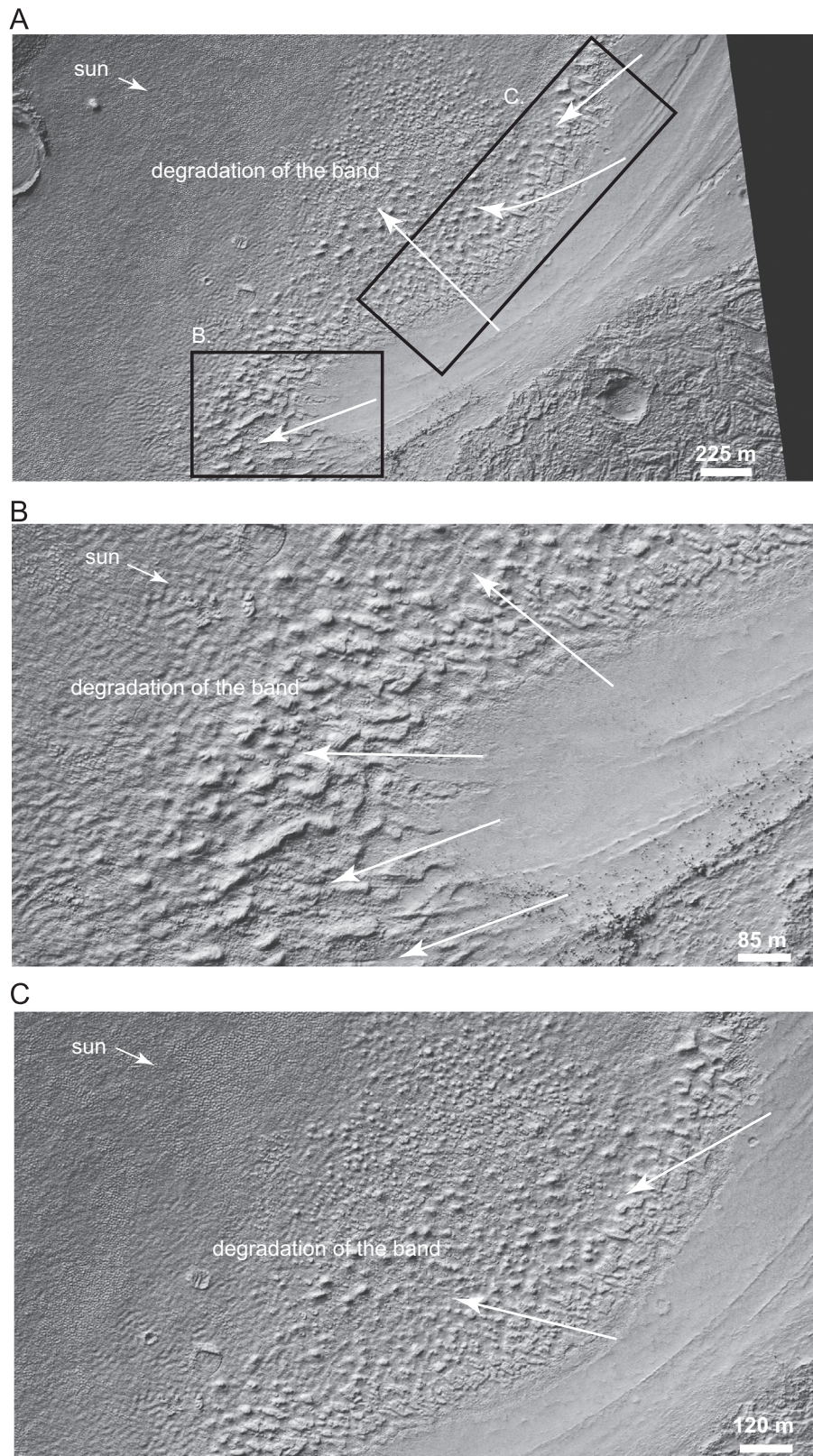


Fig. 15. HiRISE image showing the degradation of the boundaries of a linear band observed on HiRISE image (image ID: ESP_025925_1420, located at 37.8°S, 56.8°E). The degradation in distinct blocks could be due to the process of thaw–freeze of ice but also to the sublimation of ice.

a plastic flow frozen on the slope. In addition, the crater statistics and the presence of undeformed craters on the bands' surface imply that the formation of these bands was both recent and episodic.

The analysis of the morphology from high resolution images (HiRISE) reveals the presence of polygons, mounds with cracks on the top and progressive degradation of the bands, consistent with the presence, past or contemporary, of an ice rich material in the

subsurface. The banded terrain unit has been observed only in the Hellas basin to date. So the flow responsible for the formation of the banded terrain appears to be local. The interactions between honeycomb and banded terrain as well as between the different morphologies of bands, which appear to be complex, are still not well understood and need further geomorphologic investigations to completely unravel. Finally, the observations of periglacial structures (fractured mound, polygons) combined with the morphology of the bands suggest that near-surface ice flowing down slopes remains a viable hypothesis of formation for these unusual features in Hellas basin. However, the low basal stresses potentially require considering an alternative material than pure ice for the formation of the banded terrain. Such a material should be capable of flowing at low temperatures and moderate stresses on relatively gentle slopes ($< 15^\circ$).

Acknowledgments

XD would like to thank the Center for Space and Habitability of the University of Bern for funding and supporting this study. MR EM, NT, and FS are supported by funds from the Swiss National Science Foundation (SNSF). PMG is funded by the UK Space Agency (Aurora Fellowship grant ST/J005215/1). The stereo DTM processing was carried out at the UK NASA RPIF at University College London. The authors would like to thank Nicolas Mangold and an anonymous reviewer for their constructive reviews, which improved the manuscript overall.

References

- Ahnert, F., 1984. Local relief and the height limit of mountain ranges. *Am. J. Sci.* 284, 1035–1055.
- Allen P.A., Earth surface processes, *John Wiley & Sons*, 2009.
- Andrews-Hanna, J.-C., Phillips, R.-J., Zuber, M.-T., 2007. Meridiani Planum and the global hydrology of Mars. *Nature* 446, 163–166.
- Ansan, V., Loizeau, D., Mangold, N., Mouélic, S.L., Carter, J., Poulet, F., Dromart, G., Lucas, A., Bibring, J.-P., Gendrin, A., Gondet, B., Langevin, Y., Masson, P., Murchie, S., Mustard, J., Neukum, G., 2011. Stratigraphy, mineralogy, and origin of layered deposits inside Terby crater, Mars. *Icarus* 211, 273–304.
- Baioni, D., Wezel, F.C., 2010. Morphology and origin of an evaporite dome in Tithonium chasma. *Mars Planet. Space* 58, 847–857.
- Bandfield, J.L., 2008. High-silica deposits of an aqueous origin in western Hellas basin, Mars. *Geophys. Res. Lett.* 35, 12.
- Bandfield, J.L., Amador, E.S., Thomas, N.H., 2013. Extensive hydrated silica materials in western Hellas basin, Mars. *Icarus* 226, 1489–1498.
- Cantor, B.A., James, P.B., Caplinger, M., Wolff, M.J., 2001. Martian dust storms: 1999 Mars Orbiter Camera observations. *J. Geophys. Res.* 106 (E10), 23653–23687.
- Cabrol, N.A., Grin, E.A., 2010. Lakes on Mars. Elsevier, Amsterdam p. 550.
- Crown, D.A., Bleamaster, L.F., Mest, S.C., 2005. Styles and timing of volatile-driven activity in the eastern Hellas region of Mars. *J. Geophys. Res.* 110 (E12).
- Crown, D.A., Price, K.H., Greeley, R., 1992. Geologic evolution of the east rim of the Hellas basin Mars. *Icarus* 100, 1–25.
- De La Chapelle, S., Castelnaud, O., Lipendkov, V., Duval, P., 1998. Dynamic recrystallization and texture development in ice as revealed by the study of deep ice cores in Antarctica and Greenland. *J. Geophys. Res.* 103 (B3), 2091–5105.
- Diot, X., El Maarry, M., Schlunegger, F., Thomas, N., Norton, K., 2013. Geomorphological architecture of the banded terrain at the NW of Hellas basin. *Mars. Eur. Planet. Sci. Congr.* 100 (abstract #).
- Dundas, C.M., McEwen, A.S., 2010. An assessment of evidence for pingos on Mars using HiRISE. *Icarus* 205, 244–258.
- El Maarry, M.R., Markiewicz, W.J., Mellon, M.T., Goetz, W., Dohm, J.M., Pack, A., 2010. Crater floor polygons: desiccation patterns of ancient lakes on Mars? *J. Geophys. Res.* 115 (E10).
- El Maarry, M., Thomas, N., Pommerol, A., 2012a. Banded terrain and associated geology at the NW of Hellas basin, Mars. *Lunar Planet. Inst. Sci. Conf.* 2653 (abstract #).
- El Maarry, M.R., Kodikara, J., Wijessoriya, S., Markiewicz, W.J., Thomas, N., 2012b. Desiccation mechanism for formation of giant polygons on Earth and intermediate-sized polygons on Mars: Results from a pre-fracture model. *Earth Planet. Sci. Lett.* 323–324, 19–26.
- Goldsby, D., Kohlstedt, D., 1997. Flow of ice I by dislocation, grain boundary sliding, and diffusion processes. *Lunar Planet. Inst. Sci. Conf.* 429 (abstract #).
- Goldsby, D.L., Kohlstedt, D.L., 2001. Superplastic deformation of ice: experimental observations. *J. Geophys. Res.* 106 (B6), 11017–11030.
- Gorelick, N., Weiss-Malik, M., Steinberg, B., Anwar, S., 2003. JMARS: a multimission data fusion application. *Lunar Planet. Inst. Sci. Conf.* 2057 (abstract #).
- Grindrod, P.M., Fawcett, S.A., 2011. Possible climate-related signals in high-resolution topography of lobate debris aprons in Tempe Terra, Mars. *Geophys. Res. Lett.* 38, L19201, <http://dx.doi.org/10.1029/2011GL049295>.
- Grindrod, P.M., West, M., Warner, N.H., Gupta, S., 2012. Formation of an Hesperian-aged sedimentary basin containing phyllosilicates in Coprates Catena, Mars. *Icarus* 218, 178–195, <http://dx.doi.org/10.1016/j.icarus.2011.11.027>.
- Grohmann, C.H., Riccomini, C., 2009. Comparison of roving-window and search-window techniques for characterizing landscape morphometry. *Comput. Geosci.* 35, 2164–2169.
- Haberle, R.M., McKay, C.P., Schaeffer, J., Cabrol, N.A., Grin, E.A., Zent, A.P., Quinn, R., 2001. On the possibility of liquid water on present-day Mars. *J. Geophys. Res.* 106 (E10), 23317–23326.
- Hartmann, W.K., Ansan, V., Berman, D.C., Mangold, N., Forget, F., 2014. Comprehensive analysis of glaciated martian crater Greg. *Icarus* 228, 96–120.
- Harrison, K.P., Grimm, R.E., 2009. Regionally compartmented groundwater flow on Mars. *J. Geophys. Res.* 114 (E4).
- Head, J., Marchant, D., 2003. Cold-based mountain glaciers on Mars: Western Arsia Mons. *Geology* 31, 641.
- Head, J.W., et al., 2005. Tropical to mid-latitude snow and ice accumulation, flow and glaciation on Mars. *Nature* 434, 346–351, <http://dx.doi.org/10.1038/nature03359>.
- Head, J.W., et al., 2006. Extensive valley glacier deposits in the northern mid-latitudes of Mars: evidence for late Amazonian obliquity-driven climate change. *Earth Planet. Sci. Lett.* 241, <http://dx.doi.org/10.1016/j.epsl.2005.11.016>.
- Howard, A.D., Spiga, A., Moore, J.M., 2012. The deepest basin on Mars is formed by eolian erosion: Western Hellas Planitia. *LPSC 1105* (abstract).
- Hubbard, B., Milliken, R.E., Kargel, J.S., Limaye, A., Souness, C., 2011. Geomorphological characterisation and interpretation of a mid-latitude glacier-like form: Hellas Planitia, Mars. *Icarus* 211, 330–346.
- Kirk, R.L., Howington-Kraus, E., Rosiek, M.R., Anderson, J.A., Archinal, B.A., Becker, K.J., Cook, D.A., Galuszka, D.M., Geissler, P.E., Hare, T.M., Holmberg, I.M., Keszthelyi, L.P., Redding, B.L., Delamere, W.A., Gallagher, D., Chapel, J.D., Eliason, E.M., King, R., McEwen, A.S., 2008. Ultrahigh resolution topographic mapping of Mars with MRO HiRISE stereo images: meter-scale slopes of candidate Phoenix landing sites. *J. Geophys. Res.* 113 (E3).
- Kostama, V.-P., Kukkonen, S., Raitala, J., 2013. Outflow channels of Mars: formation process and timing of Waikato Vallis–Morpheus Basin–Reull Vallis–Fluvial System in the Eastern Hellas Rim Region. *Lunar Planet. Inst. Sci. Conf.* 2656 (abstract #).
- Lachenbruch, A.H., 1962. Mechanics of thermal contraction cracks and ice-wedge polygons in permafrost. *Spec. Pap. Geol. Soc. Am.* 70, 69.
- Lefort, A., Thomas, R.P., N., 2005. Ice sublimation landforms in Peneus and Amphitrites Patera. *Lunar Planet. Inst. Sci. Conf.* 1626 (abstract #).
- Lefort, A., Russell, P., Thomas, N., 2010. Scalloped terrains in the Peneus and Amphitrites Paterae region of Mars as observed by HiRISE. *Icarus* 205, 259–268.
- Levy, J.S., Head, J.W., Marchant, D.R., 2009. Concentric crater fill in Utopia Planitia: History and interaction between glacial “brain terrain” and periglacial mantle processes. *Icarus* 202, 462–476.
- Levy, J.S., Marchant, D.R., Head, J.W., 2010. Thermal contraction crack polygons on Mars: a synthesis from HiRISE, Phoenix, and terrestrial analog studies. *Icarus* 206, 229–252.
- Li, H., Robinson, M.S., Jurdy, D.M., 2005. Origin of martian northern hemisphere mid-latitude lobate debris aprons. *Icarus* 176, 382–394.
- Malin, M.C., Bell, J.F., Cantor, B.A., Caplinger, M.A., Calvin, W.M., Clancy, R.T., Edgett, K.S., Edwards, L., Haberle, R.M., James, P.B., Lee, S.W., Ravine, M.A., Thomas, P.C., Wolff, M.J., 2007. Context Camera Investigation on board the Mars reconnaissance orbiter. *J. Geophys. Res.* 112 (E5).
- Mangold, N., 2005. High latitude patterned grounds on Mars: classification, distribution and climatic control. *Icarus* 174, 336–359.
- Mangold, N., 2003. Geomorphic analysis of lobate debris aprons on Mars at Mars Orbiter camera scale: evidence for ice sublimation initiated by fractures. *J. Geophys. Res.* 108 (E4).
- Mangold, N., Allemand, P., 2001. Topographic analysis of features related to ice on Mars. *Geophys. Res. Lett.* 28, 407–410.
- Mangold, N., Allemand, P., 2003. Ductile deformation in Hellas floor: salt diapirs or crustal domes?. In: *Proceedings of the 6th International Conference on Mars* (Abstract #3047).
- Mangold, N., Adeli, S., Conway, S., Ansan, V., Langlais, B., 2012. A chronology of early Mars climatic evolution from impact crater degradation. *J. Geophys. Res.* 117.
- McEwen, A.S., et al., 2010. The High resolution imaging science experiment (HiRISE) during MRO's primary science phase (PSP). *Icarus* 205, 2–37.
- McEwen, A.S., Eliason, E.M., Bergstrom, J.W., Bridges, N.T., Hansen, C.J., Delamere, W.A., Grant, J.A., Gulick, V.C., Herkenhoff, K.E., Keszthelyi, L., Kirk, R.L., Mellon, M.T., Squyres, S.W., Thomas, N., Weitz, C.M., 2007. Mars reconnaissance orbiters high resolution imaging science experiment (HiRISE). *J. Geophys. Res.* 112 (E5).
- Mellon, M.T., 1997. Small-scale polygonal features on Mars: Seasonal thermal contraction cracks in permafrost. *J. Geophys. Res.* 102 (E11), 25617–25628.
- Mest, S.C., Crown, D.A., 2001. Geology of the Reull Vallis region, Mars. *Icarus* 153, 89–110.
- Michael, G., Neukum, G., 2010. Planetary surface dating from crater size-frequency distribution measurements: Partial resurfacing events and statistical age uncertainty. *Earth Planet. Sci. Lett.* 294 (E4), 223–229.

- Milliken, R.E., Mustard, J.F., Goldsby, D.L., 2003. Viscous flow features on the surface of Mars: observations from high-resolution Mars Orbiter Camera (MOC) images. *J. Geophys. Res.* 108 (E6).
- Moore, J.M., Edgett, K.S., 1993. Hellas Planitia, Mars: site of net dust erosion and implications for the nature of basin floor deposits. *Geophys. Res. Lett.* 20 (15), 1599–1602.
- Moore, J.M., Wilhelms, D.E., 2001. Hellas as a possible site of ancient ice-covered lakes on Mars. *Icarus* 154, 258–276.
- Moore, J.M., Wilhelms, D.E., 2007. Geologic map of part of western Hellas Planitia. Mars U.S. Geol. Survey, Sci. Investig. Map, 2953.
- Morgan III, G.A., J.W.H., Marchant, D.R., 2009. Lineated valley fill (LVF) and lobate debris aprons (LDA) in the Deuteronilus Mensae northern dichotomy boundary region, Mars: constraints on the extent, age and episodicity of Amazonian glacial events. *Icarus* 202, 22–38.
- Nimmo, F., Tanaka, K., 2005. Early crustal evolution of Mars. *Annu. Rev. Earth Planet. Sci.* 33, 133–161.
- Okubo, C.H., 2010. Structural geology of Amazonian-aged layered sedimentary deposits in southwest Candor Chasma, Mars. *Icarus* 207, 210–225, <http://dx.doi.org/10.1016/j.icarus.2009.11.012>.
- Pierce, T.L., Crown, D.A., 2003. Morphologic and topographic analyses of debris aprons in the eastern Hellas region, Mars. *Icarus* 163, 46–65.
- Plaut, J.J., et al., 2009. Radar evidence for ice in lobate debris aprons in the mid-northern latitudes of Mars. *Geophys. Res. Lett.* 36, L02203, <http://dx.doi.org/10.1029/2008GL036379>.
- Séjourné, A., Costard, F., Gargani, J., Soare, R., Fedorov, A., Marmo, C., 2011. Scalloped depressions and small-sized polygons in western Utopia Planitia, Mars: a new formation hypothesis. *Planet. Space Sci.* 59, 412–422.
- Smith, D.E., Zuber, M.T., Frey, H.V., Garvin, J.B., Head, J.W., Muhleman, D.O., Pettengill, G.H., Phillips, R.J., Solomon, S.C., Zwally, H.J., Banerdt, W.B., Duxbury, T.C., Golombek, M.P., Lemoine, F.G., Neumann, G.A., Rowlands, D.D., Aharonson, O., Ford, P.G., Ivanov, A.B., Johnson, C.L., McGovern, P.J., Abshire, J.B., Afzal, R.S., Sun, X., 2001. Mars Orbiter Laser Altimeter: experiment summary after the first year of global mapping of Mars. *J. Geophys. Res.* 106 (E10), 23689–23722.
- Smith, D.E., Zuber, M.T., Solomon, S.C., Phillips, R.J., Head, J.W., Garvin, J.B., Banerdt, W.B., Muhleman, D.O., Pettengill, G.H., Neumann, G.A., Lemoine, F.G., Abshire, J. B., Aharonson, O., David, C., Brown, Hauck, S.A., Ivanov, A.B., McGovern, P.J., Zwally, H.J., Duxbury, T.C., 1999. The global topography of Mars and implications for surface evolution. *Science* 284 (5419), 1495–1503.
- Soare, R., Conway, S., Pearce, G., Dohm, J., Grindrod, P., 2013. Possible crater-based pingos, paleolakes and periglacial landscapes at the high latitudes of Utopia Planitia, Mars. *Icarus* 225, 971–981.
- Squyres, S.W., 1979. The distribution of lobate debris aprons and similar flows on Mars. *J. Geophys. Res.* 84 (B14), 8087–8096.
- Tanaka, K.L., Leonard, G.J., 1995. Geology and landscape evolution of the Hellas region of Mars. *J. Geophys. Res.* 100 (E3), 5407–5432.
- Thomas, N., Beyer, R., Byrne, S., Moore, J., Wilson, S., Wray, J., McEwen, A., 2010. The banded terrain in the NW Region of Hellas basin. *Eur. Planet. Sci. Congr.* 338 (abstract #).
- Werner, S.C., 2008. The early martian evolution—Constraints from basin formation ages. *Icarus* 195, 45–60.
- Whalley, W.B., Martin, H.E., 1992. Rock glacier II. models and mechanisms. *Progr. Phys. Geogr.* 16 (2), 127–186.
- Wilson, S.A., Howard, A.D., Moore, J.M., Grant, J.A., 2007. Geomorphic and stratigraphic analysis of Crater Terby and layered deposits north of Hellas basin, Mars. *J. Geophys. Res.* 112 (E8).
- Wilson, S.A., Moore, J.M., Howard, A.D., Wilhelms, D.E., 2010. Evidence for ancient lakes in the Hellas region. In: Cabrol, N., Grin, E. (Eds.), *Lakes on Mars*. Elsevier, Oxford, UK, pp. 195–223.
- Zuschneid, W., van Gasselt, S., 2013. Fluvial Processes in Eastern Hellas Planitia, Mars: New Stratigraphic Insights. *Lunar Planet. Inst. Sci. Conf.* 2191 (abstracts #).

Web references

- <<http://jmars.asu.edu>>.
 <<http://www.esri.com/software/arcgis>>.
 <<http://www.bluemarblegeo.com/products/global-mapper.php>>.